GEOPHYSICS, VOL. 64, NO. 6 (NOVEMBER-DECEMBER 1999); P. 1863–1866, 2 FIGS.

Short Note

Staggered mesh for the anisotropic and viscoelastic wave equation

José M. Carcione*

INTRODUCTION

Computation of the spatial derivatives with nonlocal differential operators, such as the Fourier pseudospectral method, may cause strong numerical artifacts in the form of noncausal ringing. This situation happens when regular grids are used. The problem is attacked by using a staggered pseudospectral technique, with a different scheme for each rheological relation. The nature and causes of acausal ringing in regular grid methods and the reasons why staggered-grid methods eliminate this problem are explained in papers by Fornberg (1990) and Özdenvar and McMechan (1996). Thus, the objective here is not to propose a new method but to develop the algorithm for the viscoelastic and transversely isotropic (VTI) wave equation, for which the technique can be implemented without interpolation. The algorithm is illustrated for one physical situation that requires very high accuracy, such as a fluid-solid interface, where very large contrasts in material properties occur. The staggered-grid solution is noise free in the dynamic range where regular grids generate artifacts that may have amplitudes similar to those of physical arrivals.

THE WAVE EQUATION

The time-domain equations for propagation in a heterogeneous VTI medium can be found in Carcione (1995). The anelasticity is described by the standard linear solid, also called the Zener model, that gives relaxation and creep functions in agreement with experimental results (Zener, 1948).

The notation in Carcione (1995) denotes the relaxed or low-frequency limit stiffness coefficients as c_{IJ} and the unrelaxed or high-frequency limit stiffness coefficients as $\hat{c}_{IJ}$. To use the standard notation and define the purely elastic limit in the unrelaxed regime, we denote the unrelaxed coefficients by c_{IJ} and the relaxed coefficients by c^0_{IJ}.

The 2-D velocity-stress equations for anelastic propagation in the (x, z)-plane, assigning one relaxation mechanism to dilatational anelastic deformations ($\nu = 1$) and one relaxation mechanism to shear anelastic deformations ($\nu = 2$), can be expressed by the following equations.

First are Newton's equations:

$$\sigma_{xx,x} + \sigma_{xz,z} = \rho \dot{v}_x + f_x \tag{1}$$

and

$$\sigma_{xz,x} + \sigma_{zz,z} = \rho \dot{v}_z + f_z, \tag{2}$$

where v_x and v_z are the particle velocities; σ_{xx}, σ_{zz}, and σ_{xz} are the stress components; ρ is the density; and f_x and f_z are the body forces. A dot above a variable denotes time differentiation.

The constitutive equations are

$$\dot{\sigma}_{xx} = c_{11} v_{x,x} + c_{13} v_{z,z} + K^0 \epsilon_1 + 2c^0_{55} \epsilon_2, \tag{3}$$

$$\dot{\sigma}_{zz} = c_{13} v_{x,x} + c_{33} v_{z,z} + K^0 \epsilon_1 - 2c^0_{55} \epsilon_2, \tag{4}$$

and

$$\dot{\sigma}_{xz} = c_{55}(v_{x,z} + v_{z,x}) + c^0_{55} \epsilon_3, \tag{5}$$

where ϵ_1, ϵ_2 and ϵ_3 are memory variables. The value

$$K^0 = \tfrac{1}{2}\left(c^0_{11} + c^0_{33}\right) - c^0_{55}. \tag{6}$$

The relaxed stiffnesses are

$$c^0_{11} = c_{11} - D + K\eta_1 + c_{55}\eta_2, \tag{7}$$

$$c^0_{33} = c_{33} - D + K\eta_1 + c_{55}\eta_2, \tag{8}$$

$$c^0_{13} = c_{13} - D + K\eta_1 + c_{55}(2 - \eta_2), \tag{9}$$

and

$$c^0_{55} = c_{55}\eta_2, \tag{10}$$

with

$$K = D - c_{55}, \qquad D = \tfrac{1}{2}(c_{11} + c_{33}) \tag{11}$$

Manuscript received by the Editor December 9, 1997; revised manuscript received November 3, 1998.
*Osservatorio Geofisico Sperimentale, P.O. Box 2011 Opicina, 34016 Trieste, Italy. E-mail: jcarcione@ogs.trieste.it.

and

$$\eta_v = \frac{\tau_\sigma^{(v)}}{\tau_\epsilon^{(v)}}. \tag{12}$$

The values $\tau_\sigma^{(v)}$ and $\tau_\epsilon^{(v)}$ are material relaxation times, corresponding to dilatational and shear deformations.

The constitutive equations satisfy the condition that the mean stress depends only on the dilatational relaxation function in any coordinate system. (The trace of the stress tensor should be invariant under coordinate transformations.) Moreover, the deviatoric stresses solely depend on the shear relaxation function (Carcione, 1995).

The memory variable equations are

$$\dot\epsilon_1 = \frac{1}{\tau_\sigma^{(1)}}\left[\left(1-\eta_1^{-1}\right)(v_{x,x}+v_{z,z})-\epsilon_1\right], \tag{13}$$

$$\dot\epsilon_2 = \frac{1}{2\tau_\sigma^{(2)}}\left[\left(1-\eta_2^{-1}\right)(v_{x,x}-v_{z,z})-2\epsilon_2\right], \tag{14}$$

and

$$\dot\epsilon_3 = \frac{1}{\tau_\sigma^{(2)}}\left[\left(1-\eta_2^{-1}\right)(v_{x,z}+v_{z,x})-\epsilon_3\right]. \tag{15}$$

STAGGERED MESH AND CALCULATION OF THE SPATIAL DERIVATIVES

On a regular grid the field components and material properties are represented at each grid point, say, represented by the symbol ♠. On a staggered grid, variables and material properties are defined at half-grid points as indicated in the following mesh:

♠ ◇ ♠ ◇ ♠ ◇ ♠ ◇
△ ♣ △ ♣ △ ♣ △ ♣
♠ ◇ ♠ ◇ ♠ ◇ ♠ ◇
△ ♣ △ ♣ △ ♣ △ ♣
♠ ◇ ♠ ◇ ♠ ◇ ♠ ◇
△ ♣ △ ♣ △ ♣ △ ♣
♠ ◇ ♠ ◇ ♠ ◇ ♠ ◇

such that

$$\begin{aligned}
&\spadesuit\ (i,\ j) \quad \sigma_{xx},\ \sigma_{zz},\ \epsilon_1,\ \epsilon_2,\ c_{IJ},\ K^0,\ c_{55}^0,\ \tau_\sigma^{(v)},\ \eta_v,\\
&\diamond\ \left(i+\tfrac12,\ j\right) \quad v_x,\ f_x,\ \rho,\\
&\triangle\ \left(i,\ j+\tfrac12\right) \quad v_z,\ f_z,\ \rho,
\end{aligned} \tag{16}$$

and

$$\clubsuit\quad \left(i+\tfrac12,\ j+\tfrac12\right) \quad \sigma_{xz},\ \epsilon_3,\ c_{55},\ c_{55}^0,\ \tau_\sigma^{(2)},\ \eta_2.$$

Material properties at half-grid points ◇, ♣, and △ are computed by averaging the values defined at regular points ♠. The averaging is chosen in such a way to reduce the error between the numerical solution corresponding to an interface aligned with the numerical grid and the equivalent solution obtained with a regular grid. Minimum ringing amplitudes for the example illustrated in the next section are obtained when the averages are computed as follows. The density at points ◇ and △ is

$$\rho^{i+\frac12,j} = \frac12(\rho^{i,j}+\rho^{i+1,j}) \tag{17}$$

and

$$\rho^{i,j+\frac12} = \frac12\left(\rho^{i,j}+\rho^{i,j+1}\right), \tag{18}$$

respectively. The value c_{55} at points ♣ is

$$\left(c_{55}^{i+\frac12,j+\frac12}\right)^{-1} = \frac14\Big[\left(c_{55}^{i,j}\right)^{-1}+\left(c_{55}^{i+1,j}\right)^{-1} + \left(c_{55}^{i,j+1}\right)^{-1}+\left(c_{55}^{i+1,j+1}\right)^{-1}\Big]; \tag{19}$$

and c_{55}^0 is c_{55} (Røsten et al., 1996). The values $\tau_\sigma^{(2)}$ and η_2 are a simple arithmetic averaging of the form

$$a^{i+\frac12,j+\frac12} = \frac14(a^{i,j}+a^{i+1,j}+a^{i,j+1}+a^{i+1,j+1}). \tag{20}$$

A review of the artifacts and numerical instabilities caused by the Fourier differential operator when using a regular grid can be found in Özdenvar and McMechan (1996, 1997). As they show, the use of a staggered grid overcomes these problems. The first-order derivative computed with the staggered differential operator is evaluated between grid points and uses even-based Fourier transforms. The standard first-order differential operator along the x-direction is

$$D_x\phi = \sum_{k_X=0}^{k_X(N)} ik_x\tilde\phi(k_x)\exp(ik_xx), \tag{21}$$

where $\tilde\phi$ is the Fourier transform of ϕ and $k_x(N)$ is the Nyquist wavenumber. Staggered operators, which evaluate the derivatives between grid points, are given by

$$D_x^\pm\phi = \sum_{k_X=0}^{k_X(N)} ik_x\exp(\pm ik_x\Delta x/2)\tilde\phi(k_x)\exp(ik_xx), \tag{22}$$

where Δx is the grid spacing.

The staggered viscoelastic equations can be written as

$$\begin{aligned}
&\diamond\ D_x^+\sigma_{xx}+D_z^-\sigma_{xz} = \rho\dot v_x+f_x,\\
&\triangle\ D_x^-\sigma_{xz}+D_z^+\sigma_{zz} = \rho\dot v_z+f_z,\\
&\spadesuit\ \dot\sigma_{xx} = c_{11}D_x^-v_x+c_{13}D_z^-v_z+K^0\epsilon_1+2c_{55}^0\epsilon_2,\\
&\spadesuit\ \dot\sigma_{zz} = c_{13}D_x^-v_x+c_{33}D_z^-v_z+K^0\epsilon_1-2c_{55}^0\epsilon_2,\\
&\clubsuit\ \dot\sigma_{xz} = c_{55}\left(D_z^+v_x+D_x^+v_z\right)+c_{55}^0\epsilon_3,\\
&\spadesuit\ \dot\epsilon_1 = \frac{1}{\tau_\sigma^{(1)}}\left[\left(1-\eta_1^{-1}\right)\left(D_x^-v_x+D_z^-v_z\right)-\epsilon_1\right],\\
&\spadesuit\ \dot\epsilon_2 = \frac{1}{2\tau_\sigma^{(2)}}\left[\left(1-\eta_2^{-1}\right)\left(D_x^-v_x-D_z^-v_z\right)-2\epsilon_2\right],
\end{aligned} \tag{23}$$

and

$$\clubsuit\quad \dot\epsilon_3 = \frac{1}{\tau_\sigma^{(2)}}\left[\left(1-\eta_2^{-1}\right)\left(D_z^+v_x+D_x^+v_z\right)-\epsilon_3\right].$$

EXAMPLE

The fluid-solid interface is one of the most extreme cases where the differential operator introduces a noncausal

ringing noise, generated by discontinuities in the material properties. Consider an interface where $V_f = 1500$ m/s and $\rho_f = 1000$ kg/m^3 are the velocities and density of the fluid, respectively. The properties of the (VTI) solid half-space are $V_P = \sqrt{c_{33}/\rho} = 2000$ m/s, the vertical velocity of the compressional wave; $V_S = \sqrt{c_{55}/\rho} = 1150$ m/s, the shear velocity; $\epsilon = 0.3$ and $\delta = 0.1$ are the anisotropy parameters (Thomsen, 1986); and $\rho_f = 2000$ kg/m^3, the density. In addition, the medium is viscoelastic with quality factors $Q_P = 60$ and $Q_S = 35$. Note that the wave velocities correspond to the unrelaxed state of the medium.

We consider a regular grid of 91×91 points and a staggered grid of 88×88 points, both with a grid spacing of 20 m. Figure 1 compares the respective snapshots caused by a dilatational source located 280 m above the fluid–solid interface. As can be appreciated, the staggered differential operator does not generate the ringing. To verify that late time ringing is not generated, the time history along a vertical line perpendicular to

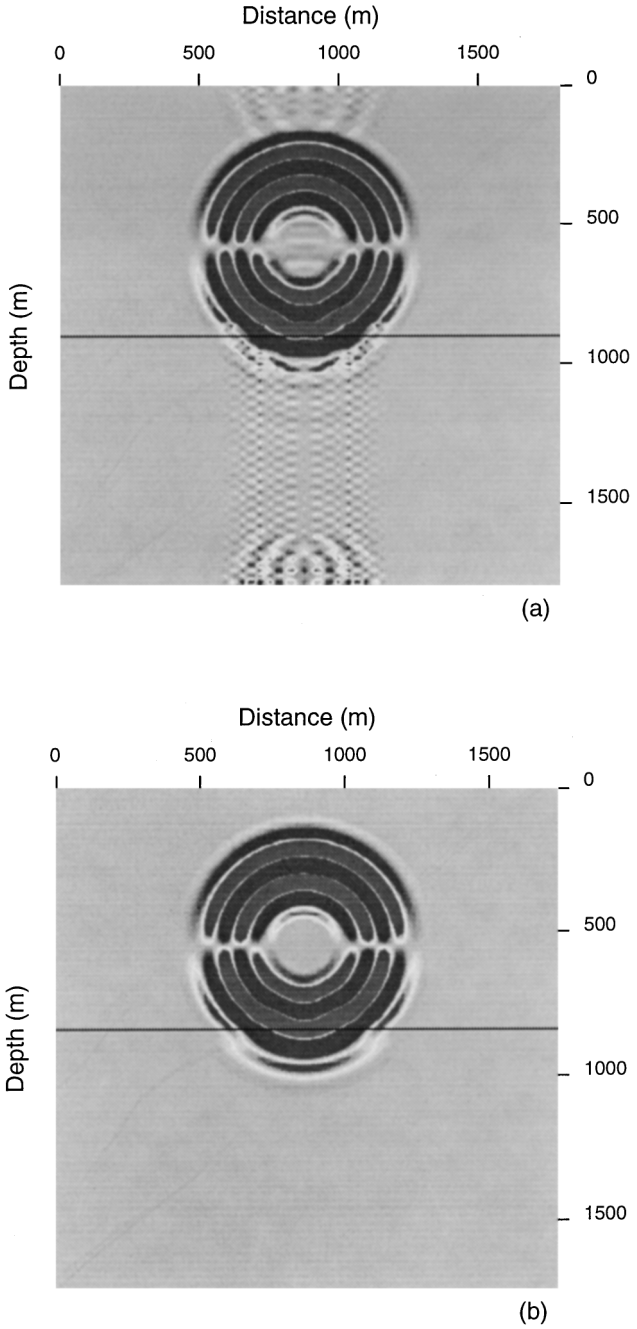

FIG. 1. Snapshot of the vertical particle velocity on (a) a regular grid and (b) a staggered grid. The source, with a central frequency of 25 Hz, is located 820 m above the fluid–solid interface. The grid size is 91×91, and the spacing is 20 m.

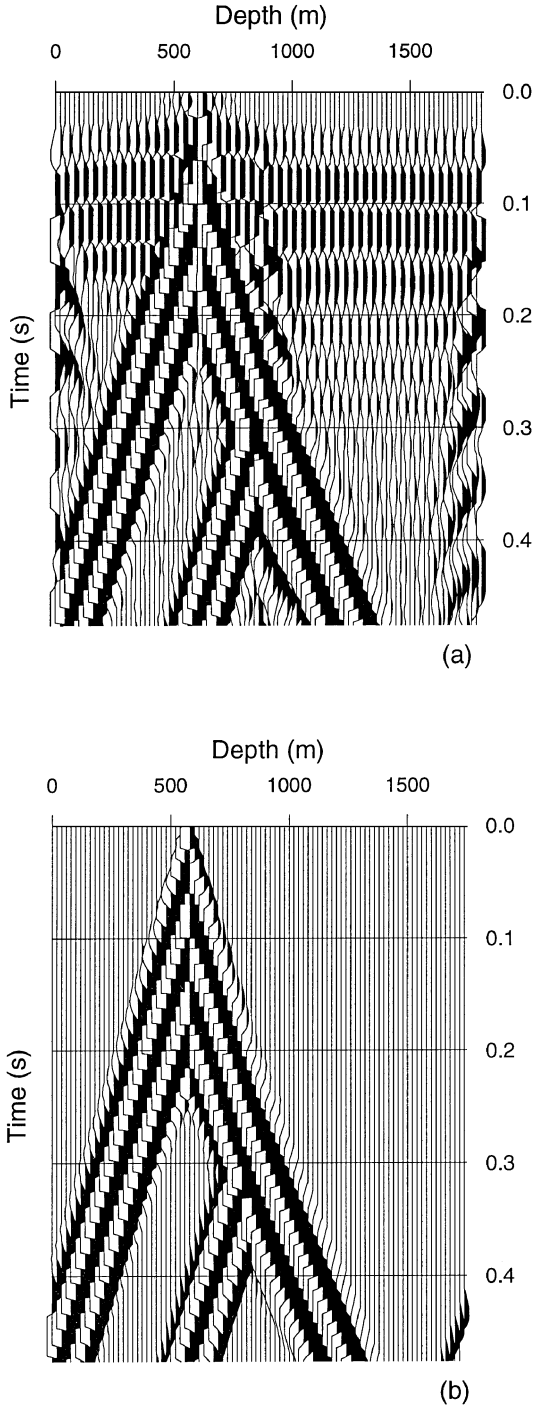

FIG. 2. Time history along a vertical line perpendicular to the fluid–solid interface, where (a) corresponds to the regular grid and (b) corresponds to the staggered grid.

the interface is illustrated in Figure 2, where (a) corresponds to the regular grid and (b) corresponds to the staggered grid. The calculations on a standard grid show strong ringing, which is not present in the staggered mesh.

ACKNOWLEDGMENTS

This work was supported in part by Norsk Hydro Bergen. Discussions with Hans B. Helle are gratefully acknowledged.

REFERENCES

Carcione, J. M., 1995, Constitutive model and wave equations for linear, viscoelastic, anisotropic media: Geophysics, **60**, 537–548.

Fornberg, B., 1990, High-order finite differences and pseudo-spectral method on staggered grids: SIAM J. Numer. Anal., **27**, 904–918.

Özdenvar, T., and McMechan, G., 1996, Causes and reduction of numerical artifacts in pseudo-spectral wavefield extrapolation: Geophys. J. Internat, **126**, 819–828.

———1997, Algorithms for staggered-grid computations for poroelastic, elastic, acoustic, and scalar wave equations: Geophys. Prosp., **45**, 403–420.

Røsten, T., Amundsen, L., Arnsten, B., and Kristensen, Å., 1996, Finite-difference modelling with application to interface wave propagation, *in* Papadakis, J. S., Ed., 3rd European Conference on Underwater Acoustics, 315–320.

Thomsen, L., 1986, Weak elastic anisotropy: Geophysics, **51**, 1954–1966.

Zener, C., 1948, Elasticity and anelasticity of metals: Univ. of Chicago Press.